Inorganic Chemistry

pubs.acs.org/IC Article

Effect of an Imidazole-Containing Schiff Base of an Aromatic Sulfonamide on the Cytotoxic Efficacy of N,N-Coordinated Half-Sandwich Ruthenium(II) *p*-Cymene Complexes

Moumita Maji, Sourav Acharya, Indira Bhattacharya, Arnab Gupta, and Arindam Mukherjee*

Cite This: *Inorg. Chem.* 2021, 60, 4744−4754 Read Online

ACCESS | Metrics & More | Article Recommendations | Supporting Information

ABSTRACT: Sulfonamides have a broad range of therapeutic applications, which include the inhibition of various isoforms of carbonic anhydrases (CAs). Among the various CA isoforms, CA IX is overexpressed in tumors and regulates the pH of the tumor microenvironment. Herein we present five new ruthenium(II) *p*-cymene complexes (**1**−**5**) of Schiff base ligands (**L1**−**L4**) of 4-(2-aminoethyl)benzenesulfonamide by varying the aldehyde to enhance the selective cytotoxicity toward cancer cells. All of the complexes are stable to aquation for the observed period of 24 h except **1**, which aquated within 1 h, but the monoaquated species is stable for 24 h. The two imidazole derivatives, **1** and **2**, are cytotoxic to the cancer cells MDA-MB-231 and MIA PaCa-2 but not to the noncancerous cells CHO and MDCK. The enhanced toxicity in hypoxia against MDA-MB-231 may be due to the greater expression of CA IX in hypoxia, as per the immunofluorescence data. The most cytotoxic complexes, **1** and **2**, are lipophilic, whereas **3**−**5** show high hydrophilicity and are not cytotoxic up to 200 μM. Complexes **1** and **2** also show a higher cellular accumulation in MDA-MB-231 than the nontoxic yet solution-stable complex **5**. The cytotoxic complexes bind with the model nucleobase 9-ethylguanine but have slow reactivity toward cellular tripeptide glutathione. Both **1** and **2** induce apoptosis by depolarizing the mitochondrial membrane potential and arrest the cell cycle in the SubG1 phase.

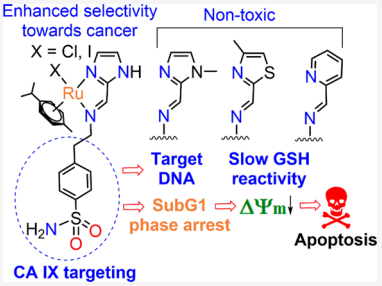

INTRODUCTION

The development of efficient metal-based anticancer agents with increased selectivity and fewer side effects is a challenging area of research.[1,2] The significant contribution of metals in anticancer therapeutics is due to the success of Pt drugs in cancer chemotherapy.[1,3−6] A wide variety of cancer treatments benefit from Pt(II) drugs, including testicular, ovarian, bladder, head and neck, and nonsmall cell lung.[7] However, Pt drugs also suffer from intrinsic or acquired resistance along with deleterious side effects.[1] Thus, the search for alternate metal-based anticancer agents has led to several Ru and Ga complexes as emerging candidates for overcoming CDDP resistance, showing a different mechanism of action.[8−11] The Ru(II) complex TLD-1433 is the first metal-based anticancer agent to enter clinical trials as a prospective PDT drug against BCG refractory high-risk invasive bladder cancer.[12] Ru(III) complexes NAMI-A and NKP1339 have shown promise in clinical trials. Although NAMI-A has not proven to be very effective and was out of the clinical trials in the recent past, NKP1339 has successfully completed phase I trials.[2,13−16] NKP1339 inhibits GRP78 and induces endoplasmic reticulum stress, leading to cell death.[17] Apart from these, organometallic Ru(II) complexes have demonstrated excellent antiproliferative activity with numerous possibilities to modulate their biological and pharmacological properties.[2,18−20] The target selectivity, stability, and pathway of action of Ru(II) complexes are modulated by the appropriate choice of ligands and the attached halide because of alteration of the steric and electronic features of the complex.[21−29]

An important property, apart from modulation of the electronic properties, is the possibility of using a ligand as an organic-directing molecule (ODM) to provide increased efficacy due to target selectivity.[24,30,31] Sulfonamides are ODMs that display a broad spectrum of biological activities, particularly as anticancer, antibacterial, and antiinflammatory agents, due to the structure-based recognition of various protein targets.[32] Their targets include dihydropteroate synthase (DHPS), cyclooxygenase-2 (COX-2),[33−36] and various isoforms of carbonic anhydrases (CAs). Acetazolamide, methazolamide, ethoxzolamide, saccharin, brinzolamide, and dorzolamide molecules inhibit CAs.[37,38] Among the various isoforms of CAs, it is now thought that CA IX and CA XII are two membrane-bound isoforms that help to control the pH of cancer cells in a hypoxic environment. Thus, hypoxia-inducible CA IX appears to be a promising target for anticancer therapy because of its overexpression in many cancer cells compared to normal cells.[39−41] The activity of CA targeting sulfonamides

Received: December 18, 2020
Published: March 24, 2021

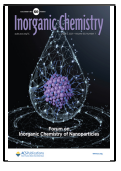

https://doi.org/10.1021/acs.inorgchem.0c03706
Inorg. Chem. 2021, 60, 4744−4754

may be modified and improved upon binding to transition-metal ions.[38,42−48] It was recently shown that 4-(2-aminoethyl)benzenesulfonamide (AEBS)-bound gold nanoparticles selectivity target CA IX over CA I and CA II.[49] Hence, sulfonamides have the scope to target cancer cells over normal cells selectively.

Hence, herein we have designed ruthenium(II) *p*-cymene complexes of four different Schiff bases with AEBS and aldehydes of imidazole, 1-methyl-2-imidazole, 4-methylthiazole, and pyridine. These N,N-donor ligands impart stability to the Ru(II) complexes, but their cytotoxicity varies enormously. We present here the stability, cytotoxicity, and pathway of action of these complexes, suggesting the importance of the imidazole motif in rendering higher cytotoxicity. In contrast, the AEBS motif provides better selectivity to cancer cells expressing CA IX.

EXPERIMENTAL SECTION

Materials and Methods. All of the chemicals were purchased from commercial sources and used without any further purification. The solvents were distilled before use using standard procedures. The metal precursor complexes $[Ru^{II}_2(\eta^6\text{-}p\text{-cymene})_2(Cl)_4]$[50] and $[Ru^{II}_2(\eta^6\text{-}p\text{-cymene})_2(I)_4]$[51] were synthesized following the literature procedures. 3-(4,5-Dimethylthiazol-2-yl)-2,5-diphenyltetrazolium bromide (MTT, USB) and other supplements were purchased from Gibco and used as received. 9-Ethylguanine (9-EtG) and glutathione (GSH) were purchased from Carbosynth and Sigma-Aldrich, respectively. Solvents for spectroscopic measurements were purchased from Merck, India. The Ru inductively coupled plasma mass spectrometry (ICP-MS) standard solution of 1000 mg L^{-1} was obtained from Sigma-Aldrich and used upon necessary dilution in 2% ultrapure nitric acid in Milli-Q water. UV−vis experiments were performed using a PerkinElmer Lambda 35 UV−vis spectrophotometer. The Fourier transform infrared (FT-IR) spectra were recorded using a PerkinElmer SPECTRUM RX I spectrometer in KBr pellets. The ^{1}H and $^{13}C\{^1H\}$ NMR spectra were recorded using either a 400 MHz JEOL ECS or a 500 MHz Bruker Avance III spectrometer at room temperature (RT; 24−27 °C). The chemical shifts of the relevant compounds are reported in parts per million (ppm). All of the mass spectra (electrospray ionization mass spectrometry, ESI-MS) were recorded in positive mode using a Bruker maXis II instrument. The isolated yields of ^{1}H NMR pure compounds are reported.

Syntheses. *(E)-4-[2-[(1H-imidazol-2-ylmethylene)amino]ethyl]-benzenesulfonamide (**L1**).* To a solution of AEBS (200 mg, 1 mmol) in 15 mL of methanol (MeOH) was added imidazole-2-carboxaldehyde (96 mg, 1 mmol), and the mixture was heated to reflux for 6 h. The product precipitated out as an off-white powder, which was washed with dichloromethane followed by diethyl ether and finally dried in a vacuum.

Yield: 223 mg, 80%. ^{1}H NMR (DMSO-d_6, 400 MHz, 298 K): δ 8.10 (s, 1H, imine-H), 7.72 (d, 2H, J = 7.6 Hz, Ar-H), 7.44 (d, 2H, J = 8.4 Hz, Ar-H), 7.27 (s, 2H, imidazole-H), 3.83 (t, 2H, J = 6.12 Hz, AEBS-CH_2), 2.99 (t, 2H, J = 6.8 Hz, AEBS-CH_2) (Figure S1). $^{13}C\{^1H\}$ NMR (DMSO-d_6, 125 MHz): δ 152.6, 144.3, 143.9, 141.9, 129.6, 129.2, 125.5, 119.2, 60.8, 36.3 (Figure S2).

*(E)-4-[2-[(1-methyl-1H-imidazol-2-ylmethylene)amino]ethyl]-benzenesulfonamide (**L2**).* To a solution of AEBS (100 mg, 0.5 mmol) in 10 mL of MeOH was added 1-methylimidazole-2-carboxaldehyde (55 mg, 0.5 mmol), and the mixture was heated to reflux for 12 h. MeOH was evaporated and the residue was dissolved in dichloromethane, which gave a pale-yellow precipitate. The residue was washed with diethyl ether and dried in a vacuum.

Yield: 190 mg, 65%. ^{1}H NMR (DMSO-d_6, 400 MHz, 298 K): δ 8.19 (s, 1H, imine-H), 7.74 (d, 2H, J = 8.4 Hz, Ar-H), 7.46 (d, 1H, J = 8.4 Hz, Ar-H), 7.28 (s, 2H, Ar-NH_2), 7.27 (s, 1H, imidazole-H), 7.00 (s, 1H, imidazole-H), 3.87 (s, 3H, imidazole N-CH_3), 3.82 (t, 2H, J = 7.0 Hz, AEBS-CH_2), 3.00 (t, 2H, J = 6.8 Hz, AEBS-CH_2) (Figure S3). $^{13}C\{^1H\}$ NMR (DMSO-d_6, 125 MHz, 298 K): δ 153.6, 144.1, 142.2, 141.9, 129.3, 128.6, 125.5, 61.7, 36.5, 34.8 (Figure S4).

*(E)-4-[2-[(1-methyl-1H-thiazol-2-ylmethylene)amino]ethyl]-benzenesulfonamide (**L3**).* To a solution of AEBS (100 mg, 0.5 mmol) in 10 mL of MeOH was added 2-methylthiazole-4-carboxaldehyde (63.5 mg, 0.5 mmol), and the mixture was heated to reflux for 12 h. MeOH was evaporated and the residue was dissolved in dichloromethane, which gave a pale-yellow precipitate. The residue was washed with diethyl ether and dried in a vacuum.

Yield: 202 mg, 65%. ^{1}H NMR (DMSO-d_6, 500 MHz, 298 K): δ 8.36 (s, 1H, imine-H), 7.73 (d, 2H, J = 8.5 Hz, Ar-H), 7.43 (d, 2H, J = 8.5 Hz, Ar-H), 7.39 (s, 1H, thiazole-H), 3.89 (t, 2H, J = 7.0 Hz, AEBS-CH_2), 3.02 (t, 2H, J = 7.0 Hz, AEBS-CH_2), 2.38 (s, 3H, thiazole-H) (Figure S5). $^{13}C\{^1H\}$ NMR (DMSO-d_6, 125 MHz, 298 K): δ 165.5, 155.6, 153.5, 143.8, 141.9, 129.3, 125.5, 117.1, 60.4, 36.0, 16.6 (Figure S6).

General Synthetic Procedure for the Preparation of Ru(II) Complexes (1−4). The complexes were synthesized according to a procedure similar to that reported by us earlier.[30] Precisely, a methanolic solution of $[Ru^{II}(p\text{-cymene})(Cl)_2]_2$ (30.5 mg, 0.05 mmol) or $[Ru^{II}(p\text{-cymene})(I)_2]_2$ (49 mg, 0.05 mmol) was added to a methanolic solution of the respective ligands (0.1 mmol) in the dark under a nitrogen atmosphere and stirred for 24 h. NH_4PF_6 (0.15 mmol) was then added and the solution stirred for another 30 min. The solvent from the resultant mixture was evaporated under reduced pressure, and the yellow solid obtained was dissolved in cold dichloromethane and filtered to remove any excess NH_4PF_6. The filtrate was evaporated, followed by washing with diethyl ether, and finally dried in a vacuum.

*$[Ru^{II}$(**L1**)(p-cymene)Cl$]PF_6$ (**1**).* Yield: 33 mg, 47%. ^{1}H NMR (DMSO-d_6, 500 MHz, 298 K): δ 8.30 (s, 1H, imine-H), 8.07 (s, 1H, imidazole-H), 7.79 (d, 2H, J = 8.0 Hz, Ar-H), 7.77 (s, 1H, imidazole-H), 7.60 (d, 2H, J = 8.0 Hz, Ar-H), 7.33 (s, 2H, Ar-NH_2), 6.29 (d, 1H, J = 6.0 Hz, *p*-cym-H), 6.06 (d, 1H, J = 6.0 Hz, *p*-cym-H), 5.99 (d, 1H, J = 6.0 Hz, *p*-cym-H), 5.77 (d, 1H, J = 6.0 Hz, *p*-cym-H), 4.64 (m, 1H, AEBS-CH_2), 4.53 (m, 1H, AEBS-CH_2), 3.39 (m, 1H, AEBS-CH_2), 3.09 (m, 1H, AEBS-CH_2), 2.61 (m, 1H, *p*-cym-iPr-H), 2.16 (s, 3H, *p*-cym-CH_3), 1.07 (d, 3H, J = 7.0 Hz, *p*-cym-iPr-CH_3), 0.91 (d, 3H, J = 7.0 Hz, *p*-cym-iPr-CH_3) (Figure S7). $^{13}C\{^1H\}$ NMR (DMSO-d_6, 125 MHz, 298 K): δ 159.1, 154.9, 142.4, 139.3, 129.2, 125.8, 125.2, 121.6, 105.1, 96.6, 85.3, 83.6, 82.4, 81.7, 60.8, 57.6, 57.3, 33.9, 30.5, 22.3, 20.9, 17.4 (Figure S8). UV−vis [MeOH; λ_{max}, nm (ε, M^{-1} cm^{-1})]: 298 (9620), 400 (996). ATR-IR (cm^{-1}): 3698 (s), 1673 (m), 1527 (s), 1437 (m), 1310 (s), 1148 (s), 684 (m). ESI-HRMS (MeOH): m/z (exp) 549.0681 (549.0660) $[Ru^{II}C_{22}H_{28}ClN_4O_2S^+]$. Elem anal. Calcd for $C_{22}H_{28}ClN_4O_2SPF_6Ru$: C, 38.07; H, 4.07; N, 8.07. Found: C, 38.15; H, 4.00; N, 8.10.

*$[Ru^{II}$(**L1**)(p-cymene)I$]PF_6$ (**2**).* Yield: 39 mg, 50%. ^{1}H NMR (DMSO-d_6, 500 MHz, 298 K): δ 8.27 (s, 1H, imine-H), 8.06 (s, 1H, imidazole-H), 7.81 (d, 2H, J = 8.0 Hz, Ar-H), 7.74 (s, 1H, imidazole-H), 7.62 (d, 2H, J = 8.0 Hz, Ar-H), 7.34 (s, 2H, Ar-NH_2), 6.17 (d, 1H, J = 6.0 Hz, *p*-cym-H), 6.04 (d, 1H, J = 6.0 Hz, *p*-cym-H), 5.97 (d, 1H, J = 6.0 Hz, *p*-cym-H), 5.84 (d, 1H, J = 6.5 Hz, *p*-cym-H), 4.56 (m, 2H, AEBS-CH_2), 3.40 (m, 1H, AEBS-CH_2), 3.20 (m, 1H, AEBS-CH_2), 2.71 (m, 1H, *p*-cym-iPr-H), 2.37 (s, 3H, *p*-cym-CH_3), 1.12 (d, 3H, J = 6.5 Hz, *p*-cym-iPr-CH_3), 0.89 (d, 3H, J = 7.0 Hz, *p*-cym-iPr-CH_3) (Figure S9). $^{13}C\{^1H\}$ NMR (DMSO-d_6, 125 MHz, 298 K): δ 154.9, 145.1, 142.5, 142.0, 129.3, 125.7, 123.2, 106.0, 100.1, 84.5, 84.1, 83.5, 82.6, 66.2, 36.6, 31.0, 22.2, 21.0, 20.0 (Figure S10). UV−vis [MeOH; λ_{max}, nm (ε, M^{-1} cm^{-1})]: 312 (10940), 430 (1136). ATR-IR (cm^{-1}): 3698 (s), 1673 (m), 1528 (s), 1447 (m), 1319 (s), 1145 (s). ESI-HRMS (MeOH): m/z (exp) 641.0004 (641.0016) $[Ru^{II}C_{22}H_{28}IN_4O_2S^+]$. Elem anal. Calcd (%) for $C_{22}H_{28}IN_4O_2SPF_6Ru$: C, 33.64; H, 3.59; N, 7.13. Found: C, 33.70; H, 3.56; N, 7.16.

*$[Ru^{II}$(**L2**)(p-cymene)Cl$]PF_6$ (**3**).* Yield: 35 mg, 50%. ^{1}H NMR (DMSO-d_6, 500 MHz, 298 K): δ 8.64 (s, 1H, imine-H), 8.05 (s, 1H, imidazole-H), 7.81 (d, 2H, J = 8.5 Hz, Ar-H), 7.72 (s, 1H, imidazole-H), 7.60 (d, 2H, J = 8.5 Hz, Ar-H), 7.34 (s, 2H, Ar-NH_2), 6.26 (d, 1H, J = 6.0 Hz, *p*-cym-H), 6.06 (d, 1H, J = 6.0 Hz, *p*-cym-H), 5.97 (d,

https://doi.org/10.1021/acs.inorgchem.0c03706
Inorg. Chem. 2021, 60, 4744−4754

1H, J = 6.0 Hz, p-cym-H), 5.77 (d, 1H, J = 6.0 Hz, p-cym-H), 4.61 (m, 1H, AEBS-CH_2), 4.47 (m, 1H, AEBS-CH_2), 3.92 (s, 3H, imidazole-N-Me), 3.39 (m, 1H, AEBS-CH_2), 3.09 (m, 1H, AEBS-CH_2), 2.59 (m, 1H, p-cym-iPr-H), 2.14 (s, 3H, p-cym-CH_3), 1.08 (d, 3H, J = 6.5 Hz, p-cym-iPr-CH_3), 0.94 (d, 3H, J = 7.0 Hz, p-cym-iPr-CH_3) (Figure S11). $^{13}C\{^1H\}$ NMR (DMSO-d_6, 125 MHz, 298 K): δ 155.1, 146.0, 142.5, 142.1, 133.0, 129.4, 126.6, 125.8, 103.8, 101.5, 84.8, 83.5, 82.9, 82.7, 65.7, 54.8, 35.5, 30.4, 22.2, 21.1, 18.2 (Figure S12). UV−vis [MeOH; λ_{max}, nm (ε, M^{-1} cm^{-1})]: 301 (10780), 400 (1376). ATR-IR (cm^{-1}): 3698 (s), 1673 (m), 1530 (s), 1428 (m), 1314 (s), 1143 (s), 721 (m), 680 (s). ESI-HRMS (MeOH): m/z (exp) 563.0824 (563.0816) [$Ru^{II}C_{23}H_{30}ClN_4O_2S^+$]. Elem anal. Calcd (%) for $C_{23}H_{30}ClN_4O_2SPF_6Ru$: C, 39.02; H, 4.27; N, 7.91. Found: C, 38.95; H, 4.22; N, 7.95.

*[Ru^{II}(**L3**)(p-cymene)Cl]PF_6 (**4**).* Yield: 37 mg, 51%. ^1H NMR (DMSO-d_6, 500 MHz, 298 K): δ 8.78 (s, 1H, imine-H), 8.11 (s, 1H, thiazole-H), 7.79 (d, 2H, J = 8.0 Hz, Ar-H), 7.59 (d, 2H, J = 8.5 Hz, Ar-H), 7.33 (s, 2H, Ar-NH_2), 6.44 (d, 2H, J = 9.0 Hz, p-cym-H), 6.03 (d, 2H, J = 10.0 Hz, p-cym-H), 4.74 (m, 1H, AEBS-CH_2), 4.58 (m, 1H, AEBS-CH_2), 3.37 (m, 1H, AEBS-CH_2), 3.07 (m, 1H, AEBS-CH_2), 2.81 (s, 3H, thiazole-CH_3), 2.61 (m, 1H, p-cym-iPr-H), 2.21 (s, 3H, p-cym-CH_3), 1.02 (d, 3H, J = 6.5 Hz, p-cym-iPr-CH_3), 0.95 (d, 3H, J = 6.0 Hz, p-cym-iPr-CH_3) (Figure S13). $^{13}C\{^1H\}$ NMR (DMSO-d_6, 125 MHz, 298 K): δ 161.8, 161.3, 155.7, 142.5, 141.9, 129.6, 125.7, 124.6, 106.4, 100.1, 86.3, 85.5, 66.4, 54.8, 34.93, 30.6, 22.1, 21.6, 17.9 (Figure S14). UV−vis [MeOH; λ_{max}, nm (ε, M^{-1} cm^{-1})]: 314 (9200), 415 (2420). ATR-IR (cm^{-1}): 3699 (s), 1528 (s), 1420 (m), 1310 (s), 1141 (s), 679 (m). ESI-HRMS (MeOH): m/z (exp) 641.0004 (641.0016) [$Ru^{II}C_{23}H_{29}ClN_3O_2S_2^+$]. Elem anal. Calcd for $C_{23}H_{29}ClN_3O_2S_2PF_6Ru$: C, 38.10; H, 4.03; N, 5.80. Found: C, 38.19; H, 4.06; N, 5.85.

Synthesis of [Ru^{II}(L4)(*p*-cymene)Cl]PF_6 (5). To a solution of AEBS (1 mmol) in 10 mL of MeOH was added 2-pyridinecarboxaldehyde (1.05 mmol), and the mixture was heated to reflux for 12 h. Then the solvent was evaporated to obtain a semisolid residue. The residue was washed twice with hexane and then dissolved in dichloromethane to remove any excess amine. The solution was filtered and the filtrate evaporated to give a yellow semisolid with 58% yield. The ligand dissociates with time, so it was reacted quickly to form a metal complex. Briefly, **L4** (29 mg, 0.1 mmol) was taken in MeOH and [Ru^{II}(p-cymene)$(Cl)_2]_2$ (30.5 mg, 0.05 mmol) was added with stirring at 27 °C for 24 h. NH_4PF_6 (0.15 mmol) was then added and stirred for another 30 min, followed by evaporation under reduced pressure. The yellow solid was dissolved in cold dichloromethane and filtered to remove any excess NH_4PF_6. The dichloromethane solution was then evaporated and the solid washed with diethyl ether and finally dried in a vacuum.

Yield: 32 mg, 45%. ^1H NMR (DMSO-d_6, 500 MHz, 298 K): δ 9.55 (d, 1H, J = 5.5 Hz, Py-H), 8.75 (s, 1H, imine-H), 8.25 (t, 1H, J = 7.5 Hz, Py-H), 8.16 (d, 1H, J = 7.5 Hz, Py-H), 7.82 (d, 1H, J = 6.0 Hz, Py-H), 7.80 (d, 2H, J = 8.0 Hz, Ar-H), 7.61 (d, 2H, J = 8.5 Hz, Ar-H), 7.34 (s, 2H, Ar-NH_2), 6.31 (d, 1H, J = 6.5 Hz, p-cym-H), 6.26 (d, 1H, J = 6.0 Hz, p-cym-H), 6.01 (d, 1H, J = 6.5 Hz, p-cym-H), 5.95 (d, 1H, J = 6.0 Hz, p-cym-H), 4.74 (m, 1H, AEBS-CH_2), 4.60 (m, 1H, AEBS-CH_2), 3.39 (m, 1H, AEBS-CH_2), 3.11 (m, 1H, AEBS-CH_2), 2.60 (m, 1H, p-cym-iPr-H), 2.19 (s, 3H, p-cym-CH_3), 1.02 (d, 3H, J = 7.0 Hz, p-cym-iPr-CH_3), 0.95 (d, 3H, J = 6.5 Hz, p-cym-iPr-CH_3) (Figure S15). $^{13}C\{^1H\}$ NMR (DMSO-d_6, 125 MHz, 298 K): δ 168.2, 156.4, 154.7, 143.0, 142.4, 140.3, 130.0, 129.3, 128.8, 126.2, 105.0, 104.1, 87.8, 85.5, 85.1, 84.5, 35.5, 30.9, 22.5, 21.9, 18.8 (Figure S16). UV−vis [MeOH; λ_{max}, nm (ε, M^{-1} cm^{-1})]: 267 (4280), 400 (656). ATR-IR (cm^{-1}): 3698 (s), 1528 (s), 1497 (m), 1317 (s), 1145 (s), 689 (m). ESI-HRMS (MeOH): m/z (exp) 560.0690 (560.0707) [$Ru^{II}C_{24}H_{29}ClN_3O_2S^+$]. Elem anal. Calcd for $C_{24}H_{29}ClN_3O_2SPF_6Ru$: C, 40.89; H, 4.15; N, 5.96. Found: C, 40.80; H, 4.12; N, 5.99.

Kinetics and Binding Studies: ^1H NMR and ESI-MS Experiments. The sample for ^1H NMR experiments (ca. 2 mM stock concentration) was prepared in a 4:1 (v/v) phosphate buffer (prepared in D_2O, 20 mM, pD 7.4, 4 mM NaCl) and N,N-dimethylformamide (DMF)-d_7. The data were recorded on either a 400 MHz JEOL ECS or a 500 MHz Bruker Avance III spectrometer. The samples for ESI-MS (ca. 100 μM stock concentration) were prepared in a 9:1 (v/v) phosphate buffer (5 mM, pH 7.4, 4 mM or 130 mM NaCl) and MeOH. HPLC-grade MeOH was used for ESI-MS sample preparation and dilution.

Cell Lines and Culture Conditions. Triple-negative human metastatic breast adenocarcinoma (MDA-MB-231), human pancreas ductal adenocarcinoma (MIA PaCa-2), Chinese hamster ovary (CHO), and Madin-Darby canine kidney (MDCK) cells were obtained from NCCS, Pune, India. The cells were grown in T75 or T25 flasks as an adherent monolayer in a 5% carbon dioxide atmosphere using a culture medium, supplemented with 10% fetal bovine serum (FBS; Gibco) and antibiotics (100 units mL^{-1} penicillin and 100 μg mL^{-1} streptomycin). MDA-MB-231 was grown in a 1:1 mixture of Dulbecco's modified Eagle medium (DMEM) with Ham's F12 nutrient mixture (i.e., DMEM/F-12), while MIA PaCa-2, CHO, and MDCK were cultured in DMEM, and all cell lines were maintained at their logarithmic phase of growth before each experiment and plated when upon reaching 70−80% confluence.

Cell Viability Assay. The growth inhibitory effect toward various cell lines (MDA-MB-231, MIA PaCa-2, CHO, and MDCK) was evaluated with the help of MTT assay. In brief, 4×10^3 cells $well^{-1}$ were seeded in 96-well microplates in respective media (200 μL) and incubated at 37 °C in a 5% carbon dioxide atmosphere. After 24 h of incubation, the media were renewed (200 μL). The compounds to be studied were added at appropriate concentrations. Each concentration was tested in triplicate. The compounds to be added were first solubilized in media containing dimethyl sulfoxide (DMSO) such that the concentration of DMSO in each well would not exceed 0.2%. The same amount of DMSO was added in the case of cell-based studies. The incubation was continued for 72 h. Upon completion of incubation with the compounds, the drug-containing media were removed and 200 μL of fresh media was added to each well, followed by treatment with 20 μL of a 1 mg mL^{-1} MTT in 1× phosphate-buffered saline (PBS; pH 7.2). This was followed by 3 h of incubation with a MTT solution at 37 °C. The media were then removed, and the resulting formazan crystals were dissolved in DMSO (200 μL). The growth inhibition of cells was analyzed by measuring the absorbance of the drug-treated wells with respect to that of untreated ones at 570 nm using a BIOTEK ELx800 plate reader. The IC_{50} values (drug concentrations responsible for 50% cell growth inhibition) were calculated by fitting nonlinear curves in *GraphPad Prism 5*, version 5.03, using a variable-slope model constructed by plotting the cell viability (%) versus the logarithm of the drug concentration (μM).

Distribution Coefficient Determination. The distribution coefficients of all of the complexes were determined by using the standard shake-flask method in a n-octanol and buffer (10 mM phosphate buffer, pH 7.4) system. The molar extinction coefficient of the complexes in n-octanol was first determined. The known concentration of the complexes was taken in n-octanol, then after shaking with phosphate buffer for 6 h at 37 °C in a BOD incubator, the concentration of the complexes remaining in the n-octanol phase was determined by a UV−vis spectrometer and subtracted from the actual concentration, which gave the concentration of the complexes in the aqueous phase. The distribution coefficients (log $D_{o/w}$) of the complexes were obtained from the ratio of the complexes present in n-octanol and the aqueous phase.

Metal Accumulation Study in MDA-MB-231 Cells by ICP-MS. In a 100 mm sterile tissue culture Petri dish, 5×10^5 numbers of MDA-MB-231 cells were seeded and grown for 48 h. Then the cells were treated with 30 μM **1**, **2**, and **5** complex solutions for an additional 12 h. Subsequently, the media were discarded, and the cells were washed using 1× PBS (pH 7.2). The cells for each sample were trypsinized and counted accurately. A 1×10^6 number of cells from each sample were centrifuged to form cell pellets. The cell pellets were washed twice by redispensing in 1× PBS (pH 7.2), followed by centrifugation. The cell pellets were then digested with 200 μL of extra pure (70%, v/v) nitric acid (Sigma-Aldrich) at 70 °C for 12 h. The digested cell suspension was diluted using Milli-Q water, and the

https://doi.org/10.1021/acs.inorgchem.0c03706
Inorg. Chem. 2021, 60, 4744−4754

Scheme 1. Synthetic Procedures for the Preparation of Ruthenium(II) *p*-Cymene Complexes[a]

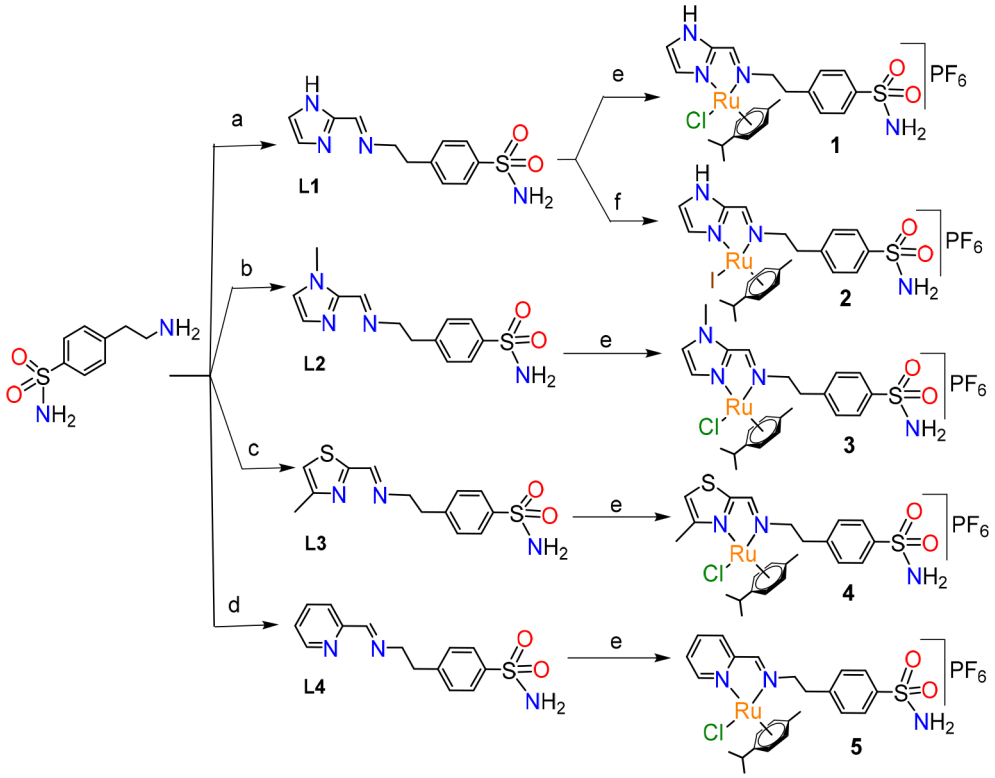

[a]Reaction conditions: (a) 2-imidazolecarboxaldehyde, MeOH, reflux, 6 h; (b) 1-methyl-2-imidazolecarboxaldehyde, MeOH, reflux, 12 h; (c) 4-methyl-2-thiazolecarboxaldehyde, MeOH, reflux, 12 h; (d) pyridine-2-carboxaldehyde, MeOH, reflux, 12 h; (e) $[Ru^{II}(\eta^6\text{-}p\text{-cymene})Cl_2]_2$, MeOH, RT, 24 h; (f) $[Ru^{II}(\eta^6\text{-}p\text{-cymene})I_2]_2$, MeOH, RT, 24 h.

Ru content in the samples was analyzed on a Thermo Scientific iCAPRQ ICP-MS instrument at the SRIC facility at Indian Institute of Technology Kharagpur. Ru standard solutions were freshly prepared to generate the calibration curve. All of the concentrations were used in triplicate to generate three independent samples, and the standard deviations were calculated.

Immunofluorescence Assay for Expression of CA IX. 1×10^4 numbers of MDA-MB-231 and MIA PaCa-2 cells were grown over glass coverslips (Corning Life Sciences) in a 6-well plate for 48 h. The cells were then fixed with 4% (w/v) paraformaldehyde in PBS for 10 min and subsequently quenched with 50 mM NH_4Cl. After washing with 1× PBS three times, the cells were blocked with 3% bovine serum albumin in PBS containing 0.1% Tween 20 (PBST) for 20 min at RT. Then the cells were incubated with a primary CA 9 antibody (abcam) 1:200 dilution for 2 h, followed by washing with 1× PBS three times. After that, the cells were incubated with a secondary antibody tagged with Alex Fluor 568 (abcam) in 1:1000 dilutions for 2 h in the dark. The cells were then washed with PBST, followed by 1× PBS. The cells were mounted on slides for imaging using a Fluoroshield mounting medium. The images were acquired in Zeiss LSM 710 and Leica SP8 confocal microscopes.

Cell Cycle Analysis. MDA-MB-231 cells, 1×10^5 per plate, were seeded in a 6-well plate in DMEM-F12 culture media and incubated at 37 °C in a 5% carbon dioxide atmosphere. After 48 h, the existing media were renewed by fresh media. Then adequate concentrations of complexes **1** and **2** were added and incubated for 24 h. After drug exposure for 24 h, the cells were harvested by quick trypsinization and washed twice with cold 1× PBS (pH 7.2). The resultant cells were resuspended in 100 μL of cold 1× PBS and fixed with 70% aqueous ethanol overnight at 4 °C. DNA staining was performed by resuspending the cell pellets in a 1× PBS solution comprised of a propidium iodide (PI; 55 $\mu g\ mL^{-1}$) and RNase A (100 $\mu g\ mL^{-1}$) solution. The cell suspension was gently mixed with a PI staining solution and incubated at 37 °C for 0.5 h. The samples were analyzed in a BD Biosciences FACS Calibur flow cytometer.

Detection of Apoptosis: Annexin V Assay. Apoptotic cells were detected using an Annexin V-PE and 7-AAD dual-staining apoptosis detection kit (BD Pharmingen) by flow cytometry according to the manufacturer's protocol. 1×10^5 cells of MDA-MB-231 were seeded a 6-well plate using 2 mL of DMEM+F-12 media. Then the cells were incubated at 37 °C in a 5% carbon dioxide atmosphere for 48 h. Subsequently, the media were changed, and the cells were treated with different concentrations of drug solutions of **1** and **2** for 24 h. The cells were then harvested by cold 1× PBS containing 0.1 mM ethylenediaminetetraacetic acid, subsequently washed twice with cold 1× PBS, and finally resuspended in an Annexin V binding buffer. The cells were then incubated with both Annexin V-PE and 7-AAD for 15 min under dark conditions at 25 °C. The data were analyzed in a BD Biosciences FACS Calibur flow cytometer within 1 h of sample preparation.

Mitochondrial Membrane Potential Determination by JC-1. Investigation of the change in the mitochondrial transmembrane potential (MMP, $\Delta\Psi_m$) was determined using flow cytometry after staining live cells with JC-1. 1×10^5 MDA-MB-231 cells were seeded in a 6-well plate. After 48 h of incubation, the media were removed and the cells treated with complex **1** or **2** using IC_{25} and IC_{50} concentrations for 24 h. The media were then removed and the cells washed with 1× PBS. The cells were then trypsinized and combined with the washing. The combined mixture was centrifuged at 2000 rpm for 4 min. The cell pellets were washed twice with 1× PBS and resuspended in 1× PBS supplemented with 10% FBS. The resultant solution was then incubated with 5 $\mu g\ mL^{-1}$ JC-1 dye for 30 min in the dark. Finally, after removal of the supernatant, the cells were suspended in 1× PBS and analyzed in a BD Bioscience FACS Calibur flow cytometer by measuring the red and green fluorescent intensities.

Reaction with NADH. The reaction of complexes **1** and **2** (ca. 2 μM) with NADH (100 μM) in 1:9 (v/v) MeOH in water was

https://doi.org/10.1021/acs.inorgchem.0c03706
Inorg. Chem. 2021, 60, 4744−4754

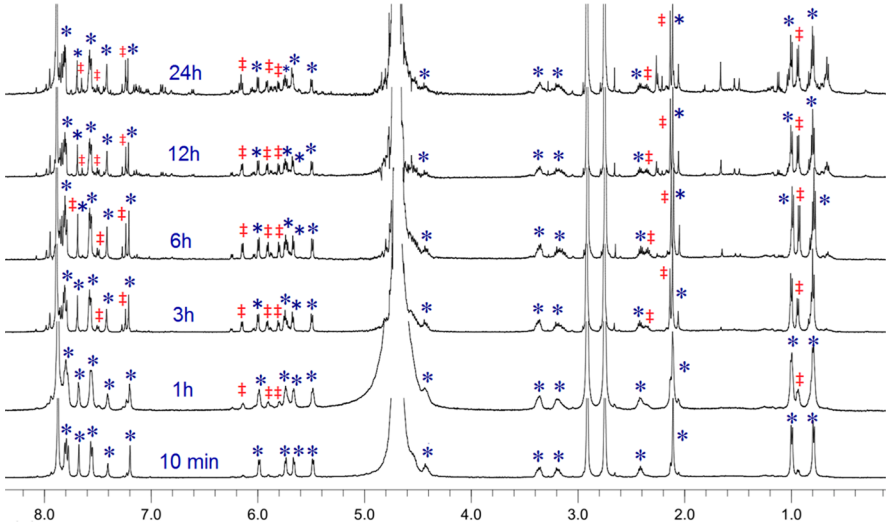

Figure 1. ^{1}H NMR spectra of the stability of **1** in 20% DMF-d_7 in a phosphate buffer (20 mM, p*D* 7.4, 4 mM NaCl): (blue *) intact complex **1**; (red ‡) aquated complex **1**.

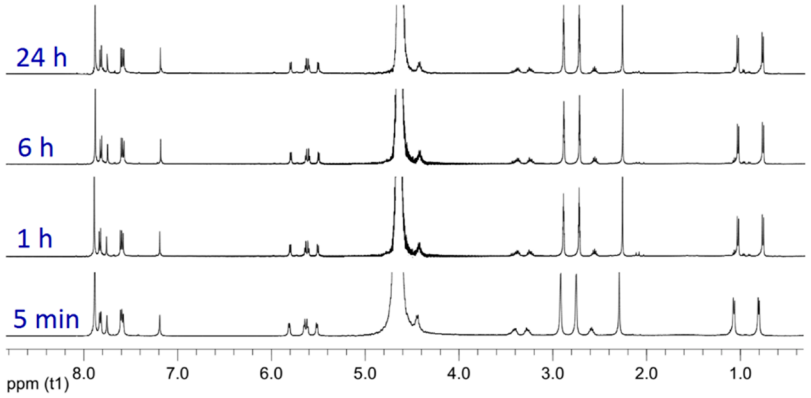

Figure 2. ^{1}H NMR spectra of the stability of **2** in 20% DMF-d_7 in a phosphate buffer (20 mM, p*D* 7.4, 4 mM NaCl) showing no hydrolysis even after 24 h.

monitored by UV−vis spectra at 298 K after various time intervals of up to 8 h. The concentration of NADH was obtained using the extinction coefficient ε_{339} = 6220 M^{-1} cm^{-1}.

RESULTS AND DISCUSSION

Syntheses and Characterizations. The sulfonamide-based N,N-chelating ligands (**L1**−**L4**) were synthesized by refluxing the respective amines and aldehydes in MeOH. The cationic complexes were isolated with hexafluorophosphate as the counteranion, making them easy to purify and less moisture-sensitive. The ligands were characterized by ^{1}H and $^{13}C\{^{1}H\}$ NMR and used to synthesize the Ru(II) complexes. The ruthenium(II) *p*-cymene complexes (**1**−**5**) were synthesized by stirring the respective ligands with $[Ru^{II}(\eta^6\text{-}p\text{-cymene})Cl_2]_2$ or $[Ru^{II}(\eta^6\text{-}p\text{-cymene})I_2]_2$ in MeOH at RT for 24 h (Scheme 1). All of the complexes herein are reported for the first time and characterized by various analytical techniques, viz., ^{1}H and $^{13}C\{^{1}H\}$ NMR, ESI-HRMS, FT-IR, and UV−vis analysis. The bulk purity of the complexes was ascertained from elemental analysis. The stretching frequency corresponding to C═N of the imine appears in the range of 1670−1675 cm^{-1} in all complexes. In the case of the ruthenium arene complexes **1**−**5**, the UV−vis spectral data in MeOH showed an intense band at around 270−315 nm that may be attributed to $\pi-\pi^*$ transitions and a relatively weak band in the 405−450 nm range corresponding to a metal-to-ligand charge-transfer transition.

Hydrolysis Study. The stability of complexes **1**−**5** in physiological conditions was investigated by ^{1}H NMR in 20% DMF-d_7 in a phosphate buffer (20 mM, p*D* 7.4, containing 4 mM NaCl). Complex **1**, bearing the imidazole motif with ruthenium chlorido coordination, starts to generate the aquated product within 1 h, and the extent of the aquation increases over time. The aquated product is stable up to the observed period of 24 h (Figure 1). The ESI-MS data support the conclusion from the above ^{1}H NMR data. ESI-MS performed in 10% MeOH containing a phosphate buffer (5 mM, pH 7.4, containing 4 mM NaCl) shows the formation of $[Ru(\mathbf{L1}\text{-}H^+)(p\text{-cymene})]^+$ species at *m*/*z* 513.0886 (calcd *m*/*z* 513.0893), supporting aquation even when both the complex concentration and percentage of the organic solvent are lower (Figures S18−S20). The **L1**-bearing, iodido-coordinated Ru(II) complex **2** did not show any aquation up to 24 h, as per the ^{1}H NMR data (Figure 2). Thus, changing the coordinated halide from chlorido to iodido made the Ru−halide bond less susceptible to aquation. The reason may be the iodido group having higher polarizability than the chlorido group introduces higher covalency in the Ru−I bond

https://doi.org/10.1021/acs.inorgchem.0c03706
Inorg. Chem. 2021, 60, 4744−4754

compared to the Ru−Cl bond. Therefore, in a polar aqueous medium, complex **2** is less susceptible to getting replaced by water and, hence, hydrolytically more stable. This is also well supported by the ESI-MS data in a phosphate buffer (5 mM, pH 7.4, containing 4 mM NaCl) containing 10% MeOH, which show a small amount of the dehalogenated adduct $[Ru(\mathbf{L1}\text{-}H^{+})(p\text{-cymene})]^{+}$, under the total spectral envelope, even after 30 h of incubation, corresponding to m/z 513.0963 (calcd m/z 513.0893) (Figures S21 and S22). In the presence of a higher chloride concentration, ca. 130 mM, slow chlorido exchange occurred, and even after 24 h, half of the intact iodido derivative **2** was present in the solution (Figures S23 and S24). The ^{1}H NMR spectra of the hydrolysis of **3** and **4**, which have the *N*-methylimidazole and 4-methylthiazole motifs, respectively, show hydrolytic stability of up to 24 h in similar experimental conditions (Figures S25 and S26). The pyridine motif bearing **5** starts aquating after 3 h with a slow increase in the aquated adduct over the observed period of 24 h (Figure S27).

Cytotoxicity. The derivatives of AEBS show excellent inhibition activity against CA IX, having K_i values ranging between 20 nM to 10 μM.[52−54] Thus, the cytotoxicities of the ligands and their metal complexes (**1**−**5**) were assessed against two cancer cells, viz., triple-negative metastatic breast adenocarcinoma (MDA-MB-231) and human pancreas ductal adenocarcinoma (MIA PaCa-2), because they are known to overexpress CA IX.[55] It is known that normal ovary and kidney cells express very low amounts of CA IX compared to MDA-MB-231 or MIA PaCa-2.[55] So, we used two noncancerous cells, viz., Chinese hamster ovary (CHO) and Madin-Darby canine kidney (MDCK), to investigate the selectivity. The free ligands (**L1**−**L3**) were not toxic up to 200 μM, and they dissociate over time in an aqueous solution to the respective amines and aldehydes. The Ru(II) complexes of the imidazole derivatives **1** and **2** showed moderate-to-good toxicity in the tested cancer cell lines in both normoxia and hypoxia (Table 1 and Figures S28 and S29). The iodido derivative **2** showed greater toxicity in MIA PaCa-2 compared to the chlorido derivative **1**, but in MDA-MB-231 cells, it is almost the same under normoxic conditions. However, under a hypoxic environment, complex **2** showed a better cytotoxic efficacy compared to **1**. Surprisingly the Ru(II) complexes **3**−**5** were also not toxic up to 200 μM, although they have the same sulfonamide motif just condensed with different aldehydes. This may be because of their higher solution stability in physiological conditions because most complexes of this type are known to act by aquation of the Ru−halide bond, followed by binding to the nucleophilic target (viz., DNA).[56,57]

Table 1. Cytotoxicity of Complexes 1 and 2 against Several Cancerous and Noncancerous Cells

	$IC_{50} \pm SD$ (μM)[a]				
	normoxia				hypoxia
complex	CHO	MDCK	MIA PaCa-2	MDA-MB-231	MDA-MB-231
1	>200	>200	22.5 ± 1.5	38.3 ± 1.5	27.9 ± 1.0
2	>200	>200	17.1 ± 1.0	39.6 ± 3.2	17.7 ± 1.8

[a]$IC_{50} \pm SD$ (SD = standard deviation) is determined by MTT assay in normoxia (~12% O_2) and hypoxia (~1.5% O_2) as a means of at least three independent experiments. In a single experiment, each concentration was assayed in triplicate. The statistical significance (P) of the IC_{50} data ranges between >0.001 and <0.05.

The cytotoxicity of both imidazole analogues **1** and **2** improved in the hypoxic condition in MDA-MB-231. The gain of cytotoxicity in hypoxia is encouraging because many cancer drugs become less efficient in hypoxia. Furthermore, complexes **1** and **2** are not cytotoxic toward the noncancerous CHO and MDCK cells up to 200 μM (Table 1 and Figure S30). This implies that incorporation of the sulfonamide moiety as part of the ligand framework improved the selectivity. Despite the known literature stating that CA IX is overexpressed under hypoxia in MDA-MB-231,[58] we needed to confirm the same under our experimental conditions. Thus, we carried out immunofluorescence studies of overexpression of CA IX in normoxia and hypoxia in MDA-MB-231 and MIA PaCa-2. The results show that both cell lines express CA IX (Figure 3).

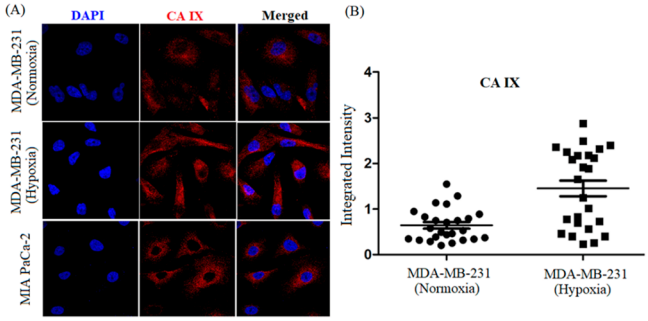

Figure 3. (A) Immunofluorescence study showing CA IX expression in MDA-MB-231 cells in normoxia, MDA-MB-231 cells in hypoxia, and MIA PaCa-2 cells in hypoxia. CA IX was visualized with a monoclonal anti-CA IX antibody interacting with a secondary antibody tagged with Alex Fluor 568 (λ_{em} = 603 nm). (B) Integrated intensity of CA IX expression in MDA-MB-231 cells in normoxia and hypoxia.

Furthermore, the immunofluorescence images suggest that the expression of CA IX in MDA-MB-231 might have increased in hypoxia, unlike MIA PaCa-2 (Figure 3A), which has similar CA IX expressions in both normoxia and hypoxia. This apparent increase in expression may be responsible for the marginal enhancement in the cytotoxicity in hypoxia in MDA-MB-231 (Figure 3B).

Lipophilicity and Cellular Accumulation. Lipophilicity is a parameter for drug uptake, primarily via passive diffusion.[59] The lipophilicity is often measured by the distribution coefficient of a drug between the organic and aqueous phases. We have measured the lipophilicity of **1**−**5** to see if there is any correlation between lipophilicity, cellular uptake, and cytotoxicity. The distribution coefficient of the complexes was measured by the shake-flask method in an *n*-octanol/phosphate buffer (pH 7.4) mixture. Distribution coefficient data suggest that the imidazole analogues (**1** and **2**) are more lipophilic compared to the *N*-methylimidazole-, thiazole-, and pyridine-based complexes (**3**−**5**). The imidazole analogue **2** having iodido as part of the leaving group is the most lipophilic (log $D_{o/w}$ of ca. 0.92) in the series, followed by the chlorido analogue **1** (log $D_{o/w}$ of ca. 0.06). In contrast, the rest of the three complexes (**3**−**5**) show more hydrophilicity, with the distribution coefficient values ranging from ca. −0.54 to −1.32 (Figure 4A). Complexes **1** and **2**, being most lipophilic in the series, may better enter the cancer cells through passive diffusion and hence are the most cytotoxic. However, despite

https://doi.org/10.1021/acs.inorgchem.0c03706
Inorg. Chem. 2021, 60, 4744−4754

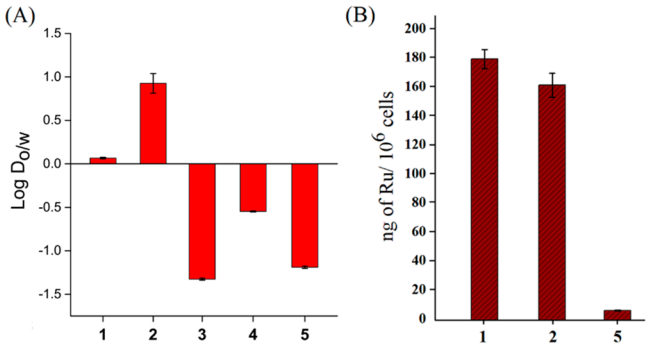

Figure 4. (A) Lipophilicities of complexes **1**−**5** in an *n*-octanol/buffer mixture. (B) Cellular accumulation of complexes **1**, **2**, and **5** in MDA-MB-231 cells after incubation for 12 h.

having a large difference in hydrophobicity between **1** and **2**, we have found that there is only a marginal difference in cytotoxicity in MIA PaCa-2 and almost no difference in the MDA-MB-231 cells in normoxia. To understand this, we have done cellular accumulation by measuring the total Ru content (ng of Ru per 10^6 cells) of **1** and **2** along with complex **5** with relatively high hydrophilicity. The ICP-MS data show that **1** and **2** accumulate in similar amounts in the MDA-MB-231 cells (Figure 4B), which correlates with their in vitro cytotoxicity. However, complex **5** shows very low accumulation in the MDA-MB-231 cells compared to **1** and **2** (Figure 4B); hence, it is nontoxic. The similar cytotoxicities of **1** and **2** in spite of their different lipophilicities indicate that there may be a receptor-mediated uptake or the iodido is exchanged to chlorido in solution because we have observed slow iodido exchange in ESI-MS in a 5 mM phosphate buffer having 130 mM NaCl (Figures S23 and S24). The poor cytotoxicity of complexes **3**−**5** may be ascribed to the combination of reduced interaction with CA IX and the relatively high hydrophilicity, which prevents passive diffusion-based uptake, resulting in poor accumulation, as supported by the ICP-MS cellular accumulation data of **5** (Figure 4B). In our earlier studies, the pyridine-2-aldehyde-based complexes display low cellular accumulation.[30] The present work is also supportive of the same. Thus, the overall structural effect, including lipophilicity, influenced by the presence of an imidazole moiety (a free −NH group) plays an important role in cytotoxicity, making complexes **1** and **2** the most cytotoxic among the series, which is also found in our previous reports.[30] Hence, the imidazole-containing AEBS ligand along with the relatively stable Ru−I coordination makes complex **2** the most optimum among the studied complexes.

Mechanism of Cell Killing. Complexes **1** and **2** were further investigated for a mechanistic study. The MDA-MB-231 cells treated with **1** and **2** were investigated for their cell cycle arrest by measuring the DNA content using flow cytometry. Treatment with IC_{25} and IC_{50} concentrations of **1** and **2** for 24 h showed cell cycle arrest mostly in the SubG1 phase (Figure 5A). The Annexin V-PE/7-AAD dual-staining study in MDA-MB-231 also supported the apoptotic pathway of cell killing. Complex **1** induced 11−24% apoptosis, whereas **2** induced 24−42% apoptosis at the IC_{25} and IC_{50} dosages (Figures 5B and S31). We next investigated alteration of the mitochondrial membrane potential and found that **1** and **2** affect the mitochondrial membrane potential. They depolarize the mitochondrial membrane, changing the red fluorescence (λ_{em} = 590 nm) of the cationic dye JC-1 to green fluorescence (λ_{em} = 550 nm) because of breaking of the J-aggregates of the dye. The flow cytometry data showed that the depolarization was 4 times higher than the control experiment without the complexes (Figure 5C). Depolarization of the mitochondria suggests that the intrinsic pathway of apoptosis may be favored by these complexes. It has been shown that NADH can donate a hydride to aquairidium(III) cyclopentadienyl or ruthenium(II) arene complexes and produce reactive oxygen species.[31,60] Our investigations with complexes **1** and **2** show that they do not induce oxidative stress by disruption of the NADH to NAD^+ redox balance inside the cells. This was confirmed by treating **1** and **2** with NADH in 1:9 (v/v) MeOH and water containing 4 mM NaCl. The absorption recorded at λ_{max} of 260 and 340 nm for 8 h showed no significant change in intensity compared to the control (Figure S32), suggesting that the complexes could not convert NADH to NAD^+.

Binding with 9-EtG and GSH. The cytotoxic complexes **1** and **2** were studied for their binding ability with 9-EtG by either ^{1}H NMR or ESI-MS. 9-EtG was used as the model nucleobase because it mimics well the N^7 of guanine, which is a well-known target for similar metal complexes.[61] The N^7 of guanine is the favored binding position, and a downfield chemical shift of the H8 immediate next to N^7 is observed in ^{1}H NMR upon binding with the metal center. The ^{1}H NMR spectra of **1** with 2 mol equiv of 9-EtG in 1:4 (v/v) DMF-d_7 in

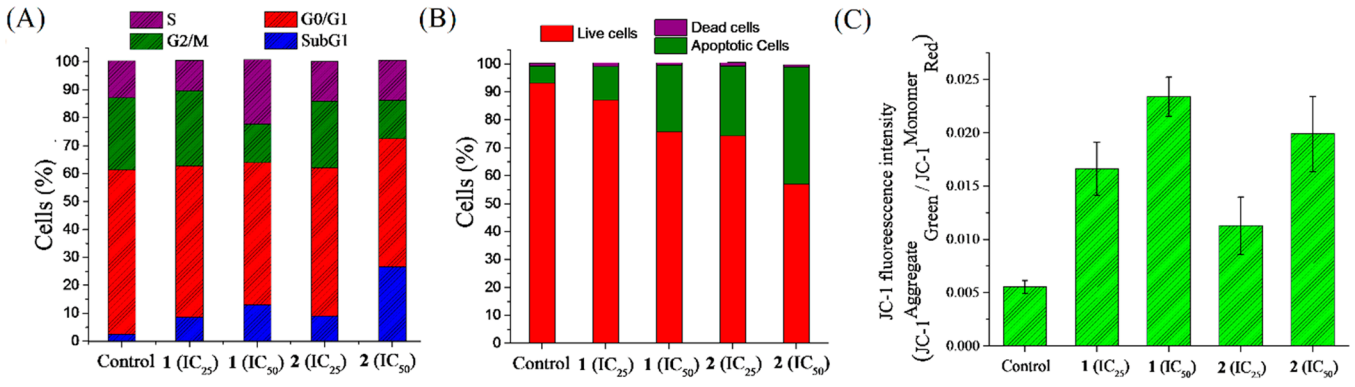

Figure 5. (A) Cell cycle distribution of **1** and **2** in the MDA-MB-231 cell line after treatment with the IC_{25} and IC_{50} dosages for 24 h. (B) Induction of apoptosis with the IC_{25} and IC_{50} dosages of **1** and **2** for 24 h in the MDA-MB-231 cells by flow cytometry analysis using Annexin V-PE/7-AAD dual staining. (C) Change in the mitochondrial membrane potential in the MDA-MB-231 cells after treatment with the IC_{25} and IC_{50} concentrations of **1** and **2** for 24 h.

https://doi.org/10.1021/acs.inorgchem.0c03706
Inorg. Chem. 2021, 60, 4744−4754

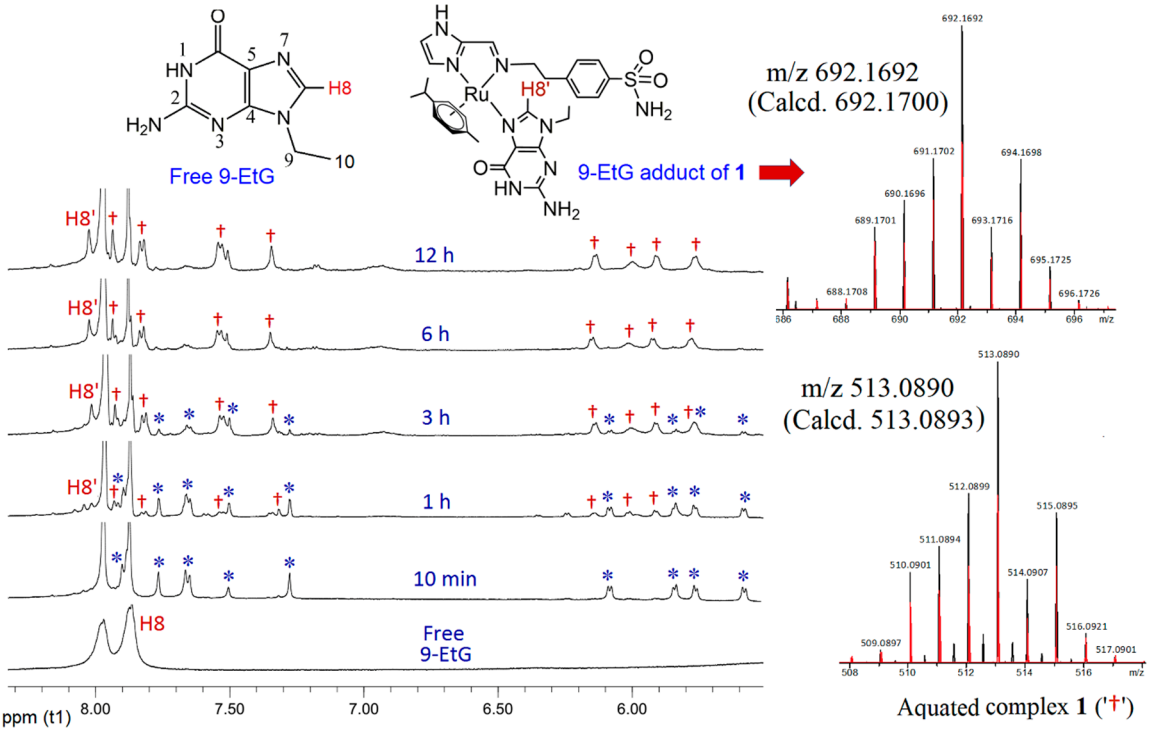

Figure 6. ^{1}H NMR spectra of the interaction of 9-EtG with complex **1** in 20% DMF-d_7 in a phosphate buffer (20 mM, p*D* 7.4, 4 mM NaCl): (blue *) intact complex **1**; (red †) aquated complex **1**. H8′ indicates the chemical shift of the 9-EtG proton (H8) after binding.

a phosphate buffer (20 mM, p*D* 7.4, containing 4 mM NaCl) show formation of the 9-EtG adduct within 1 h, as shown by the shift of the H8 proton of 9-EtG from 7.75 to 8.05 ppm (marked as H8′; Figure 6). After 24 h, the 9-EtG adduct predominates in the solution along with the hydrolyzed complex **1**. This finding is also supported by the ESI-MS data, where even at a much lower concentration of the complex (ca. 100 μM), the behavior toward 9-EtG adduct formation is similar. The 9-EtG adduct forms at m/z 692.1707 (calcd m/z 692.1700) corresponding to the formulation $[(\mathbf{1} - H^+ - Cl^-) + 9\text{-EtG}]^+$ (Figures S33 and S34). Complex **2** also shows formation of the 9-EtG adduct at m/z 692.1693 (calcd m/z 692.1700) having the formulation $[(\mathbf{2} - H^+ - I^-) + 9\text{-EtG}]^+$ (Figures S35 and S36). Thus, the Ru complexes **1** and **2** may be able to target cellular DNA.

GSH is a cellular tripeptide that remains abundant in most cancer cells and is thought to be one of the major cellular components responsible for the deactivation of Pt and other metallodrugs.[62,63] The ruthenium(II) *p*-cymene complexes also efficiently react with GSH or oxidize in the presence of GSH.[61,64] In our earlier reports, the N,N-coordinated ruthenium *p*-cymene complexes show excellent GSH resistance.[65] Hence, complexes **1** and **2** were also studied for their binding ability with GSH by ESI-MS. The ESI-MS spectra of **1** with 2 equiv of GSH in 10% MeOH in a phosphate buffer (5 mM, pH 7.4, containing 4 mM NaCl) show only a small amount of the GSH adduct after 3 h at m/z 820.1739 (calcd m/z 820.1731) corresponding to the formulation $[(\mathbf{1} - Cl^-) + (GSH - H^+)]^+$, which increases slowly over time up to the observed period of 24 h (Figures S37 and S38). On the other hand, in the case of **2**, the extent of formation of the GSH adduct is less than 1. Even after 24 h, the majority of the intact complex and the aquated adduct are present in the solution (Figures S39 and S40). Thus, complex **1** and especially complex **2** have a lower affinity to bind with GSH.

CONCLUSIONS

The N,N-chelating half-sandwich ruthenium(II) *p*-cymene complexes containing sulfonamide and imidazole moieties showed cytotoxicity in triple-negative breast cancer cells MDA-MB-231 and pancreatic cancer cells MIA PaCa-2 but not toward the noncancerous CHO and MDCK cell lines. They show a marginal enhancement in the toxicity in hypoxia against MDA-MB-231. The enhancement in the toxicity in hypoxia is more prominent for the ruthenium iodido complex **2** compared to the ruthenium chlorido complex **1**. Complexes **3**−**5** are not cytotoxic; thus, functionalization of CA IX-inhibiting AEBS with the respective aldehydes and formation of their metal complexes alter the electronic properties and structural recognition of the complexes. The selectivity of complexes **1** and **2** may not be solely due to CA IX expression because the complexes are lipophilic, so they may also enter inside the cells through passive diffusion, yet they are selective to certain forms of cancer, which is highly encouraging. They induce apoptosis by depolarizing the mitochondrial membrane potential and arrest the cell cycle in the SubG1 phase. The complexes efficiently bind with 9-EtG and possess slower reactivity toward thiol. Hence, the sulfonamide- and imidazole-based ruthenium(II) *p*-cymene complexes altogether provide a desirable methodology to impart selectivity and warrant further studies by designing more efficient complexes with variation of the CA IX-inhibiting motif.

ASSOCIATED CONTENT

Supporting Information

The Supporting Information is available free of charge at https://pubs.acs.org/doi/10.1021/acs.inorgchem.0c03706.

https://doi.org/10.1021/acs.inorgchem.0c03706
Inorg. Chem. 2021, 60, 4744−4754

NMR spectra of ligands (Figures S1−S6) and complexes (Figures S7−S16), UV−vis spectra of the complexes (Figure S17), ESI-MS and ^{1}H NMR spectra of hydrolysis of the complexes in a buffer (Figures S18−S27), MTT assay (Figures S28−S30), different pathways of cell killing by the complexes (Figures S31 and S32), and ESI-MS spectra of 9-EtG and GSH binding of the complexes in buffer (Figures S33−S40) (PDF)

AUTHOR INFORMATION

Corresponding Author

Arindam Mukherjee − *Department of Chemical Sciences and Centre for Advanced Functional Materials, Indian Institute of Science Education and Research (IISER) Kolkata, Mohanpur 741246, West Bengal, India;* orcid.org/0000-0001-9545-8628; Email: a.mukherjee@iiserkol.ac.in

Authors

Moumita Maji − *Department of Chemical Sciences and Centre for Advanced Functional Materials, Indian Institute of Science Education and Research (IISER) Kolkata, Mohanpur 741246, West Bengal, India;* orcid.org/0000-0003-3440-0881

Sourav Acharya − *Department of Chemical Sciences and Centre for Advanced Functional Materials, Indian Institute of Science Education and Research (IISER) Kolkata, Mohanpur 741246, West Bengal, India;* orcid.org/0000-0001-5511-1312

Indira Bhattacharya − *Department of Biological Sciences, Indian Institute of Science Education and Research (IISER) Kolkata, Mohanpur 741246, West Bengal, India*

Arnab Gupta − *Department of Biological Sciences, Indian Institute of Science Education and Research (IISER) Kolkata, Mohanpur 741246, West Bengal, India*

Complete contact information is available at: https://pubs.acs.org/10.1021/acs.inorgchem.0c03706

Author Contributions

The manuscript has been submitted with the consent of all authors. The outline of the work was planned by M.M and A.M. Synthesis, characterizations, hydrolysis, binding studies by ^{1}H NMR and ESI-MS, and in vitro cytotoxicity studies were done by M.M. The mechanistic studies were jointly done by M.M. and S.A. The microscopy studies of the CA IX expression were done by I.B. All of the work was done under the supervision of A.G. and A.M.

Notes

The authors declare no competing financial interest.

ACKNOWLEDGMENTS

The authors earnestly acknowledge CSIR, Government of India, for support through Project 01(2927)/18/EMR-II. M.M. and I.B. thank CSIR and S.A. thanks UGC for their research fellowships. A.G. is thankful for an Early Career Research Award from DST, Government of India (Award ECR/2015/000220), and a Wellcome Trust-DBT India Alliance Fellowship (IA/I/16/1/502369). All of the authors thank IISER Kolkata for infrastructural and financial support. We also thank Tamal Ghosh for helping us in the flow cytometry analysis.

REFERENCES

(1) Kenny, R. G.; Marmion, C. J. Toward Multi-Targeted Platinum and Ruthenium Drugs-A New Paradigm in Cancer Drug Treatment Regimens? *Chem. Rev.* **2019**, *119*, 1058−1137.

(2) Thota, S.; Rodrigues, D. A.; Crans, D. C.; Barreiro, E. J. Ru(II) Compounds: Next-Generation Anticancer Metallotherapeutics? *J. Med. Chem.* **2018**, *61*, 5805−5821.

(3) Rosenberg, B.; VanCamp, L.; Trosko, J. E.; Mansour, V. H. Platinum compounds: a new class of potent antitumor agents. *Nature* **1969**, *222*, 385−6.

(4) Johnstone, T. C.; Park, G. Y.; Lippard, S. J. Understanding and improving platinum anticancer drugs - phenanthriplatin. *Anticancer Res.* **2014**, *34*, 471−476.

(5) Anthony, E. J.; Bolitho, E. M.; Bridgewater, H. E.; Carter, O. W. L.; Donnelly, J. M.; Imberti, C.; Lant, E. C.; Lermyte, F.; Needham, R. J.; Palau, M.; Sadler, P. J.; Shi, H.; Wang, F.-X.; Zhang, W.-Y.; Zhang, Z. Metallodrugs are unique: opportunities and challenges of discovery and development. *Chem. Sci.* **2020**, *11*, 12888−12917.

(6) Boros, E.; Dyson, P. J.; Gasser, G. Classification of Metal-Based Drugs according to Their Mechanisms of Action. *Chem.* **2020**, *6*, 41−60.

(7) Florea, A.-M.; Buesselberg, D. Cisplatin as an anti-tumor drug: cellular mechanisms of activity, drug resistance and induced side effects. *Cancers* **2011**, *3*, 1351−1371.

(8) Clarke, M. J.; Zhu, F.; Frasca, D. R. Non-Platinum Chemotherapeutic Metallopharmaceuticals. *Chem. Rev.* **1999**, *99*, 2511−2533.

(9) Zeng, L.; Gupta, P.; Chen, Y.; Wang, E.; Ji, L.; Chao, H.; Chen, Z.-S. The development of anticancer ruthenium(ii) complexes: from single molecule compounds to nanomaterials. *Chem. Soc. Rev.* **2017**, *46*, 5771−5804.

(10) Chitambar, C. R. Gallium-containing anticancer compounds. *Future Med. Chem.* **2012**, *4*, 1257−1272.

(11) Timerbaev, A. R. Advances in developing tris(8-quinolinolato)-gallium(III) as an anticancer drug: critical appraisal and prospects. *Metallomics* **2009**, *1*, 193−198.

(12) Monro, S.; Colon, K. L.; Yin, H.; Roque, J.; Konda, P.; Gujar, S.; Thummel, R. P.; Lilge, L.; Cameron, C. G.; McFarland, S. A. Transition Metal Complexes and Photodynamic Therapy from a Tumor-Centered Approach: Challenges, Opportunities, and Highlights from the Development of TLD1433. *Chem. Rev.* **2019**, *119*, 797−828.

(13) Hartinger, C. G.; Zorbas-Seifried, S.; Jakupec, M. A.; Kynast, B.; Zorbas, H.; Keppler, B. K. From bench to bedside - preclinical and early clinical development of the anticancer agent indazolium trans-[tetrachlorobis(1H-indazole)ruthenate(III)] (KP1019 or FFC14A). *J. Inorg. Biochem.* **2006**, *100*, 891−904.

(14) Trondl, R.; Heffeter, P.; Kowol, C. R.; Jakupec, M. A.; Berger, W.; Keppler, B. K. NKP-1339, the first ruthenium-based anticancer drug on the edge to clinical application. *Chem. Sci.* **2014**, *5*, 2925−2932.

(15) Improved reaction conditions for the synthesis of new NKP1339 derivatives and preliminary investigations on their anticancer potential. Kuhn, P.-S.; Pichler, V.; Roller, A.; Hejl, M.; Jakupec, M. A.; Kandioller, W.; Keppler, B. K. *Dalton Trans* **2015**, *44*, 659−68.

(16) Rilak Simovic, A.; Masnikosa, R.; Bratsos, I.; Alessio, E. Chemistry and reactivity of ruthenium(II) complexes: DNA/protein binding mode and anticancer activity are related to the complex structure. *Coord. Chem. Rev.* **2019**, *398*, 113011.

(17) Flocke, L. S.; Trondl, R.; Jakupec, M. A.; Keppler, B. K. Molecular mode of action of NKP-1339 - a clinically investigated ruthenium-based drug - involves ER- and ROS-related effects in colon carcinoma cell lines. *Invest. New Drugs* **2016**, *34*, 261−268.

(18) Meier-Menches, S. M.; Gerner, C.; Berger, W.; Hartinger, C. G.; Keppler, B. K. Structure-activity relationships for ruthenium and osmium anticancer agents - towards clinical development. *Chem. Soc. Rev.* **2018**, *47*, 909−928.

(19) Inhibition of cancer cell growth by ruthenium(II) arene complexes. Morris, R. E.; Aird, R. E.; del Socorro Murdoch, P.; Chen, H.; Cummings, J.; Hughes, N. D.; Parsons, S.; Parkin, A.; Boyd, G.; Jodrell, D. I.; Sadler, P. J. Inhibition of Cancer Cell Growth by Ruthenium(II) Arene Complexes. *J. Med. Chem.* **2001**, *44*, 3616−3621.
(20) Nowak-Sliwinska, P.; van Beijnum, J. R.; Casini, A.; Nazarov, A. A.; Wagnieres, G.; van den Bergh, H.; Dyson, P. J.; Griffioen, A. W. Organometallic Ruthenium(II) Arene Compounds with Antiangiogenic Activity. *J. Med. Chem.* **2011**, *54*, 3895−3902.
(21) Ronconi, L.; Sadler, P. J. Using coordination chemistry to design new medicines. *Coord. Chem. Rev.* **2007**, *251*, 1633−1648.
(22) Romero-Canelon, I.; Salassa, L.; Sadler, P. J. The Contrasting Activity of Iodido versus Chlorido Ruthenium and Osmium Arene Azo- and Imino-pyridine Anticancer Complexes: Control of Cell Selectivity, Cross-Resistance, p53 Dependence, and Apoptosis Pathway. *J. Med. Chem.* **2013**, *56*, 1291−1300.
(23) Pantic, D. N.; Arandelovic, S.; Radulovic, S.; Roller, A.; Arion, V. B.; Grguric-Sipka, S. Synthesis, characterisation and cytotoxic activity of organoruthenium(II)-halido complexes with 1H-benzimidazole-2-carboxylic acid. *J. Organomet. Chem.* **2016**, *819*, 61−68.
(24) Acharya, S.; Maji, M.; Ruturaj; Purkait, K.; Gupta, A.; Mukherjee, A. Synthesis, Structure, Stability, and Inhibition of Tubulin Polymerization by Ru(II)-p-Cymene Complexes of Trimethoxyaniline-Based Schiff Bases. *Inorg. Chem.* **2019**, *58*, 9213−9224.
(25) Maji, M.; Acharya, S.; Maji, S.; Purkait, K.; Gupta, A.; Mukherjee, A. Differences in Stability, Cytotoxicity, and Mechanism of Action of Ru(II) and Pt(II) Complexes of a Bidentate N,O Donor Ligand. *Inorg. Chem.* **2020**, *59*, 10262−10274.
(26) Romero-Canelon, I.; Pizarro, A. M.; Habtemariam, A.; Sadler, P. J. Contrasting cellular uptake pathways for chlorido and iodido iminopyridine ruthenium arene anticancer complexes. *Metallomics* **2012**, *4*, 1271−1279.
(27) Kurzwernhart, A.; Kandioller, W.; Baechler, S.; Bartel, C.; Martic, S.; Buczkowska, M.; Muehlgassner, G.; Jakupec, M. A.; Kraatz, H.-B.; Bednarski, P. J.; Arion, V. B.; Marko, D.; Keppler, B. K.; Hartinger, C. G. Structure-Activity Relationships of Targeted RuII(η6-p-Cymene) Anticancer Complexes with Flavonol-Derived Ligands. *J. Med. Chem.* **2012**, *55*, 10512−10522.
(28) Chelopo, M. P.; Pawar, S. A.; Sokhela, M. K.; Govender, T.; Kruger, H. G.; Maguire, G. E. M. Anticancer activity of ruthenium(II) arene complexes bearing 1,2,3,4-tetrahydroisoquinoline amino alcohol ligands. *Eur. J. Med. Chem.* **2013**, *66*, 407−414.
(29) Arshad, J.; Hanif, M.; Movassaghi, S.; Kubanik, M.; Waseem, A.; Sohnel, T.; Jamieson, S. M. F.; Hartinger, C. G. Anticancer Ru(η6-p-cymene) complexes of 2-pyridinecarbothioamides: A structure-activity relationship study. *J. Inorg. Biochem.* **2017**, *177*, 395−401.
(30) Acharya, S.; Ghosh, S.; Maji, M.; Parambil, A. R. U.; Singh, S.; Mukherjee, A. Inhibition of 3D colon cancer stem cell spheroids by cytotoxic RuII-p-cymene complexes of mesalazine derivatives. *Chem. Commun. (Cambridge, U. K.)* **2020**, *56*, 5421−5424.
(31) Tian, Z.; Li, J.; Zhang, S.; Xu, Z.; Yang, Y.; Kong, D.; Zhang, H.; Ge, X.; Zhang, J.; Liu, Z. Lysosome-Targeted Chemotherapeutics: Half-Sandwich Ruthenium(II) Complexes That Are Selectively Toxic to Cancer Cells. *Inorg. Chem.* **2018**, *57*, 10498−10502.
(32) Apaydin, S.; Torok, M. Sulfonamide derivatives as multi-target agents for complex diseases. *Bioorg. Med. Chem. Lett.* **2019**, *29*, 2042−2050.
(33) Woods, D. D. The biochemical mode of action of the sulfonamide drugs. *J. Gen. Microbiol.* **1962**, *29*, 687−702.
(34) Henry, R. J. The Mode of Action of Sulfonamides. *Bacteriol. Rev.* **1943**, *7*, 175−262.
(35) Gajraj, N. M. COX-2 inhibitors celecoxib and parecoxib: valuable options for postoperative pain management. *Curr. Top. Med. Chem.* **2007**, *7*, 235−249.
(36) Shi, S.; Klotz, U. Clinical use and pharmacological properties of selective COX-2 inhibitors. *Eur. J. Clin. Pharmacol.* **2008**, *64*, 233−252.
(37) Supuran, C. T. Carbonic anhydrases: novel therapeutic applications for inhibitors and activators. *Nat. Rev. Drug Discovery* **2008**, *7*, 168−181.
(38) Sersen, S.; Traven, K.; Kljun, J.; Turel, I.; Supuran, C. T. Organoruthenium(II) complexes of acetazolamide potently inhibit human carbonic anhydrase isoforms I, II, IX and XII. *J. Enzyme Inhib. Med. Chem.* **2019**, *34*, 388−393.
(39) Alterio, V.; Vitale, R. M.; Monti, S. M.; Pedone, C.; Scozzafava, A.; Cecchi, A.; De Simone, G.; Supuran, C. T. Carbonic Anhydrase Inhibitors: X-ray and Molecular Modeling Study for the Interaction of a Fluorescent Antitumor Sulfonamide with Isozyme II and IX. *J. Am. Chem. Soc.* **2006**, *128*, 8329−8335.
(40) Winum, J.-Y.; Rami, M.; Scozzafava, A.; Montero, J.-L.; Supuran, C. Carbonic anhydrase IX: a new druggable target for the design of antitumor agents. *Med. Res. Rev.* **2008**, *28*, 445−463.
(41) Jung, H. S.; Han, J.; Shi, H.; Koo, S.; Singh, H.; Kim, H.-J.; Sessler, J. L.; Lee, J. Y.; Kim, J.-H.; Kim, J. S. Overcoming the Limits of Hypoxia in Photodynamic Therapy: A Carbonic Anhydrase IX-Targeted Approach. *J. Am. Chem. Soc.* **2017**, *139*, 7595−7602.
(42) Loughrey, B. T.; Williams, M. L.; Healy, P. C.; Innocenti, A.; Vullo, D.; Supuran, C. T.; Parsons, P. G.; Poulsen, S.-A. Novel organometallic cationic ruthenium(II) pentamethylcyclopentadienyl benzenesulfonamide complexes targeted to inhibit carbonic anhydrase. *JBIC, J. Biol. Inorg. Chem.* **2009**, *14*, 935−945.
(43) Salmon, A. J.; Williams, M. L.; Innocenti, A.; Vullo, D.; Supuran, C. T.; Poulsen, S.-A. Inhibition of carbonic anhydrase isozymes I, II and IX with benzenesulfonamides containing an organometallic moiety. *Bioorg. Med. Chem. Lett.* **2007**, *17*, 5032−5035.
(44) Takashima, H.; Fukuda, M.; Nakagaki, F.; Ogata, T.; Tsukahara, K. Photoinduced Electron-Transfer Reactions of Carbonic Anhydrase Inhibitor Containing Tris(2,2′-bipyridine)ruthenium(II) Analogue. *J. Phys. Chem. B* **2013**, *117*, 2625−2635.
(45) Monnard, F. W.; Heinisch, T.; Nogueira, E. S.; Schirmer, T.; Ward, T. R. Human Carbonic Anhydrase II as a host for piano-stool complexes bearing a sulfonamide anchor. *Chem. Commun.* **2011**, *47*, 8238−8240.
(46) Kemp, S. A.; Prior, T. J.; Savoie, H.; Boyle, R. W.; Murray, B. S. The application of reversible intramolecular sulfonamide ligation to modulate reactivity in organometallic ruthenium(II) diamine complexes. *Molecules* **2020**, *25*, 244.
(47) Arshad, J.; Hanif, M.; Zafar, A.; Movassaghi, S.; Tong, K. K. H.; Reynisson, J.; Kubanik, M.; Waseem, A.; Soehnel, T.; Jamieson, S. M. F.; Hartinger, C. G. Organoruthenium and Organoosmium Complexes of 2-Pyridinecarbothioamides Functionalized with a Sulfonamide Motif: Synthesis, Cytotoxicity and Biomolecule Interactions. *ChemPlusChem* **2018**, *83*, 612−619.
(48) Cao, Q.; Zhou, D.-J.; Pan, Z.-Y.; Yang, G.-G.; Zhang, H.; Ji, L.-N.; Mao, Z.-W. CAIXplatins: Highly Potent Platinum(IV) Prodrugs Selective Against Carbonic Anhydrase IX for the Treatment of Hypoxic Tumors. *Angew. Chem., Int. Ed.* **2020**, *59*, 18556−18562.
(49) Stiti, M.; Cecchi, A.; Rami, M.; Abdaoui, M.; Barragan-Montero, V.; Scozzafava, A.; Guari, Y.; Winum, J.-Y.; Supuran, C. T. Carbonic Anhydrase Inhibitor Coated Gold Nanoparticles Selectively Inhibit the Tumor-Associated Isoform IX over the Cytosolic Isozymes I and II. *J. Am. Chem. Soc.* **2008**, *130*, 16130−16131.
(50) Bennett, M.; Huang, T. N.; Matheson, T.; Smith, A.; Ittel, S.; Nickerson, W. (η^6-Hexamethylbenzene) ruthenium Complexes; *Inorganic Syntheses* **2007**, *21*, 74−78.
(51) Dougan, S. J.; Habtemariam, A.; McHale, S. E.; Parsons, S.; Sadler, P. J. Catalytic organometallic anticancer complexes. *Proc. Natl. Acad. Sci. U. S. A.* **2008**, *105*, 11628−11633.
(52) Berrino, E.; Angeli, A.; Zhdanov, D. D.; Kiryukhina, A. P.; Milaneschi, A.; De Luca, A.; Bozdag, M.; Carradori, S.; Selleri, S.; Bartolucci, G.; Peat, T. S.; Ferraroni, M.; Supuran, C. T.; Carta, F. Azidothymidine "Clicked" into 1,2,3-Triazoles: First Report on Carbonic Anhydrase-Telomerase Dual-Hybrid Inhibitors. *J. Med. Chem.* **2020**, *63*, 7392−7409.

https://doi.org/10.1021/acs.inorgchem.0c03706
Inorg. Chem. 2021, 60, 4744−4754

(53) Andring, J. T.; Fouch, M.; Akocak, S.; Angeli, A.; Supuran, C. T.; Ilies, M. A.; McKenna, R. Structural Basis of Nanomolar Inhibition of Tumor-Associated Carbonic Anhydrase IX: X-Ray Crystallographic and Inhibition Study of Lipophilic Inhibitors with Acetazolamide Backbone. *J. Med. Chem.* **2020**, *63*, 13064−13075.
(54) Abdel-Aziz, A. A. M.; Angeli, A.; El-Azab, A. S.; Abu El-Enin, M. A.; Supuran, C. T. Synthesis and biological evaluation of cyclic imides incorporating benzenesulfonamide moieties as carbonic anhydrase I, II, IV and IX inhibitors. *Bioorg. Med. Chem.* **2017**, *25*, 1666−1671.
(55) Mahalingam, S. M.; Chu, H.; Liu, X.; Leamon, C. P.; Low, P. S. Carbonic Anhydrase IX-Targeted Near-Infrared Dye for Fluorescence Imaging of Hypoxic Tumors. *Bioconjugate Chem.* **2018**, *29*, 3320−3331.
(56) Peacock, A. F. A.; Melchart, M.; Deeth, R. J.; Habtemariam, A.; Parsons, S.; Sadler, P. J. Osmium(II) and ruthenium(II) arene maltolato complexes: rapid hydrolysis and nucleobase binding. *Chem. - Eur. J.* **2007**, *13*, 2601−2613.
(57) Kljun, J.; Bytzek, A. K.; Kandioller, W.; Bartel, C.; Jakupec, M. A.; Hartinger, C. G.; Keppler, B. K.; Turel, I. Physicochemical Studies and Anticancer Potency of Ruthenium η6-p-Cymene Complexes Containing Antibacterial Quinolones. *Organometallics* **2011**, *30*, 2506−2512.
(58) Robertson, N.; Potter, C.; Harris, A. L. Role of carbonic anhydrase IX in human tumor cell growth, survival, and invasion. *Cancer Res.* **2004**, *64*, 6160−6165.
(59) Arnott, J. A.; Planey, S. L. The influence of lipophilicity in drug discovery and design. *Expert Opin. Drug Discovery* **2012**, *7*, 863−875.
(60) Betanzos-Lara, S.; Liu, Z.; Habtemariam, A.; Pizarro, A. M.; Qamar, B.; Sadler, P. J. Organometallic Ruthenium and Iridium Transfer-Hydrogenation Catalysts Using Coenzyme NADH as a Cofactor. *Angew. Chem., Int. Ed.* **2012**, *51*, 3897−3900.
(61) Chen, F.; Romero-Canelon, I.; Soldevila-Barreda, J. J.; Song, J.-I.; Coverdale, J. P. C.; Clarkson, G. J.; Kasparkova, J.; Habtemariam, A.; Wills, M.; Brabec, V.; Sadler, P. J. Transfer Hydrogenation and Antiproliferative Activity of Tethered Half-Sandwich Organoruthenium Catalysts. *Organometallics* **2018**, *37*, 1555−1566.
(62) Galluzzi, L.; Senovilla, L.; Vitale, I.; Michels, J.; Martins, I.; Kepp, O.; Castedo, M.; Kroemer, G. Molecular mechanisms of cisplatin resistance. *Oncogene* **2012**, *31*, 1869−1883.
(63) De Luca, A.; Parker, L. J.; Ang, W. H.; Rodolfo, C.; Gabbarini, V.; Hancock, N. C.; Palone, F.; Mazzetti, A. P.; Menin, L.; Morton, C. J.; Parker, M. W.; Lo Bello, M. L.; Dyson, P. J. A structure-based mechanism of cisplatin resistance mediated by glutathione transferase P1−1. *Proc. Natl. Acad. Sci. U. S. A.* **2019**, *116*, 13943−13951.
(64) Petzold, H.; Sadler, P. J. Oxidation induced by the antioxidant glutathione (GSH). *Chem. Commun.* **2008**, 4413−4415.
(65) Purkait, K.; Ruturaj; Mukherjee, A.; Gupta, A. ATP7B Binds Ruthenium(II) p-Cymene Half-Sandwich Complexes: Role of Steric Hindrance and Ru-I Coordination in Rescuing the Sequestration. *Inorg. Chem.* **2019**, *58*, 15659−15670.

https://doi.org/10.1021/acs.inorgchem.0c03706
Inorg. Chem. 2021, 60, 4744−4754